IEEE Access
Multidisciplinary | Rapid Review | Open Access Journal

Received December 23, 2020, accepted January 6, 2021, date of publication January 11, 2021, date of current version January 25, 2021.

Digital Object Identifier 10.1109/ACCESS.2021.3050751

Analytical Synthesis of High-Pass, Band-Pass and Low-Pass Biquadratic Filters and Its Quadrature Oscillator Application Using Current-Feedback Operational Amplifiers

SAN-FU WANG[1], HUA-PIN CHEN[2], YITSEN KU[3], AND MING-XIU ZHONG[2]
[1]Department of Electronic Engineering, National Chin-Yi University of Technology, Taichung 41170, Taiwan, R.O.C.
[2]Department of Electronic Engineering, Ming Chi University of Technology, New Taipei 24301, Taiwan, R.O.C.
[3]Department of Electrical Engineering, California State University Fullerton, Fullerton, California, CA 92831, USA

Corresponding author: Hua-Pin Chen (hpchen@mail.mcut.edu.tw)

ABSTRACT In this paper, a method of realizing voltage-mode (VM) non-inverting high-pass filter (HPF), band-pass filter (BPF), low-pass filter (LPF), and inverting low-pass filter (ILPF) transfer functions structure with two grounded capacitors and four resistors through an analytical synthesis method is presented. The synthesis structure of the VM biquadratic filter consists of a voltage proportional block and two voltage lossless integrators based on the use of current feedback operational amplifiers (CFOAs). It is demonstrated that the derived biquadratic filter structure can simultaneously realize VM HPF, BPF and ILPF transfer functions or VM BPF and LPF transfer functions at a high-input impedance terminal. The VM biquadratic filter can independently adjust the resonance angular frequency and quality factor. By slightly modifying the proposed biquadratic filter, a VM quadrature sinusoidal oscillator can be achieved. The proposed biquadratic filter and quadrature oscillator have been simulated by OrCAD PSpice and appropriate hardware has been implemented with AD844-type CFOAs. In order to reduce power consumption, reduce chip area, reduce costs, and improve system integration, integrated VM CFOA-based biquadratic filter circuits and quadrature oscillator circuits are very important. The proposed filter and quadrature oscillator have been further fabricated in 0.18 μm 1P6M CMOS process technology. The entire chip area is 0.974 mm^2, including a filter chip cell and an oscillator chip cell. Under the supply voltage of $\pm$0.9 V, the total power dissipation of the filter chip cell is 5.4 mW, and the figure-of-merit (FOM) of filter chip cell is 66.7%. The measured value of the third-order intermodulation distortion of the filter chip cell is $-$55.29 dBc and the third-order intercept point is 19.9 dBm. The measured phase noise of CFOA-based filter chip cell at 1 kHz offset is less than $-$99.76 dBc/Hz.

INDEX TERMS CMOS, filter, oscillator, integrated circuit, current conveyor.

I. INTRODUCTION

Due to the flexibility and versatility of active filters [1]–[7] and oscillators [8]–[14] in practical applications, people are increasingly interested in their design. Active components have been recognized by circuit design researchers and have drawn great attention in realizing filters and oscillators [15]–[25]. Many studies in the literature have focused on improving the performance of voltage-mode (VM) biquadratic filters based on current feedback operational amplifier (CFOA) [26]–[40]. Of particular interest here are VM multifunction biquadratic filters based on CFOA [41]–[46]. In [41], a VM biquadratic filter is proposed, which includes three CFOAs, two grounded capacitors and three resistors. The circuit cannot enjoy high-input impedance at its input terminal, so that it is not suitable for cascading in VM operation. In [42], another VM biquadratic filter is proposed, which includes three CFOAs, three grounded capacitors and four resistors. The filter has high-input impedance, which makes the filter suitable for cascading in VM operation. However, the X ports of the CFOAs are not directly connected to the resistors, so that its performance

The associate editor coordinating the review of this manuscript and approving it for publication was Venkata Rajesh Pamula.

is not good at high frequency. In [43], a VM biquadratic filter is proposed, which includes four CFOAs, two grounded capacitors and four resistors. In [44], another VM biquadratic filter is also proposed, which includes three CFOAs, two capacitors and four resistors. However, the characteristic parameters of resonance angular frequency (ω_o) and quality factor (Q) of these two filters cannot be controlled independently. In [45], a CFOA-based VM biquadratic filter is proposed, which includes three CFOAs, two grounded capacitors and three resistors. The filter can simultaneously obtain three transfer functions, but the characteristic parameters of ω_o and Q are not independently controllable. In 2020, a satisfactory VM multifunction biquadratic filter is proposed. The filter includes three CFOAs, two capacitors and four resistors. The characteristic parameters ω_o and Q are independently controllable. The previously works [41]–[46] did not provide a systematic and structural method for realizing CFOA-based VM multifunction biquadratic filter, and did not implement the filter on a chip.

This study developed a method of realizing VM multifunction biquadratic filter structure based on three CFOAs, two grounded capacitors and four resistors. The proposed circuit simultaneously realizes VM non-inverting high-pass filter (HPF), band-pass filter (BPF) and inverting low-pass filter (ILPF) transfer functions or VM BPF and non-inverting low-pass filter (LPF) transfer functions, employs two grounded capacitors attractive for integrated circuit (IC) technology implementation and able to absorb shunt parasitic capacitances, has high-input impedance suitable for cascading, and converts into a VM quadrature sinusoidal oscillator easily. The proposed VM biquadratic filter and quadrature oscillator have been simulated by OrCAD PSpice and the appropriate hardware has been implemented with AD844-type CFOAs. Since AD844-type CFOA devices and the discrete passive components on breadboard will generate a lot of power consumption, it is important to integrate VM CFOA-based filter and oscillator on a CMOS IC, which can lower the power consumption, speed up the circuit, and improve the figure-of-merit (FOM) of the proposed filter and oscillator. Therefore, the proposed VM CFOA-based biquadratic filter and quadrature oscillator were implemented on Taiwan Semiconductor Manufacturing Company (TSMC) using 0.18 μm level-49 1P6M CMOS processing technology. The CFOA-based chip has been verified by a network analyzer and a spectrum analyzer. Table 1 compares the proposed filter with recently reported VM CFOA-based multifunction biquadratic filters [41]–[46]. As Table 1 indicates, the proposed biquadratic filter enjoys all the main advantages and realizes the biquadratic filter on chip using 0.18 μm 1P6M CMOS process technology.

To the best knowledge of the authors, there is no high-input impedance biquadratic filter based on using 0.18 μm 1P6M CMOS process CFOA-based IC, with ILPF, LPF, BPF and HPF transfer functions [26]–[46]. Multifunction filter circuits that use LPF, BPF and HPF transfer functions simultaneously have been applied in the high fidelity 3-way speaker systems, touch-tone telephone systems and phase-locked loop frequency modulation stereo demodulators etc. [16], [30], [32], [38], [47]. An attractive feature of VM CFOA-based circuit with high-input impedance in this research is that the biquadratic ILPF, BPF and HPF transfer functions or the biquadratic BPF and LPF transfer functions can be simultaneously implemented on-chip. Compared with using the off-the-shelf CFOA-type AD844 ICs, the realization based on the CMOS CFOA biquadratic filter chip cell has obtained better characteristics verification.

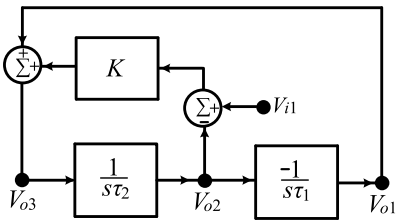

FIGURE 1. The first block diagram based on two-integrator loop VM multifunction biquadratic filter.

II. ANALYTICAL SYNTHESIS

A. VM BIQUADRATIC HPF TRANSFER FUNCTION FOR ANALYSIS AND SYNTHESIS OF SYSTEM STRUCTURE

The VM transfer function of a biquadratic HPF can often be described by

$$\frac{V_{o3}}{V_{i1}} = \frac{ks^2}{s^2 + s\frac{k}{\tau_2} + \frac{1}{\tau_1\tau_2}} \tag{1}$$

where τ_1 and τ_2 are the integrator time constants, k is a proportional gain, V_{i1} is the first input signal and V_{o3} is the third output signal.

Equation (1) can be simplified as follows:

$$[1 + \frac{k}{s\tau_2} + (\frac{1}{s\tau_1})(\frac{1}{s\tau_2})]V_{o3} = kV_{i1} \tag{2}$$

Equation (2) can be equivalent to

$$V_{o3} + k(\frac{1}{s\tau_2})V_{o3} - (\frac{-1}{s\tau_1})(\frac{1}{s\tau_2})V_{o3} = kV_{i1} \tag{3}$$

Let

$$V_{o2} = \frac{1}{s\tau_2}V_{o3} \tag{4}$$

Equation (3) is then simplified as

$$V_{o3} + kV_{o2} - (\frac{-1}{s\tau_1})V_{o2} = kV_{i1} \tag{5}$$

Let

$$V_{o1} = \frac{-1}{s\tau_1}V_{o2} \tag{6}$$

Equation (5) can be simplified again as

$$V_{o3} + kV_{o2} - V_{o1} = kV_{i1} \tag{7}$$

TABLE 1. Performance parameters of the previously reported CFOA-based filters.

Parameter	[41]	[42]	[43]	[44]	[45]	[46]	This work filter	
							Using AD844 ICs	Using CFOA-based filter chip cell
Number of CFOAs used	3	3	4	3	3	3	3	3
Passive components used	$3R$+$2C$	$4R$+$3C$	$4R$+$2C$	$4R$+$2C$	$3R$+$2C$	$4R$+$2C$	$4R$+$2C$	$4R$+$2C$
Kinds of filter functions simultaneously	3	3	4	3	3	3	3	3
Only two grounded capacitors used	yes	no	yes	yes	yes	yes	yes	yes
All the X ports of CFOAs directly connected to resistors	yes	no	yes	no	yes	yes	yes	yes
Input voltage at high-input impedance	no	yes	yes	yes	yes	yes	yes	yes
Independent tunability of ω_o and Q	no	no	no	no	no	yes	yes	yes
Easily transform into a quadrature oscillator	none	none	none	none	yes	yes	yes	yes
Analytical synthesis structure	none	none	none	none	none	none	yes	yes
Technology	AD844 ICs	AD844 ICs	AD844 ICs	AD844 ICs	AD844 ICs	AD844 ICs	AD844 ICs	CMOS 0.18 μm
Power supply (V)	N/A	N/A	N/A	±12	±6	±6	±6	±0.9
Power consumption (mW)	N/A	N/A	N/A	N/A	180	168	168	5.4
Simulation or/and Measured results	Measured	Simulation	Both	Simulation	Both	Both	Both	Both
Center frequency (kHz)	15.91	3.18	7.96	5.68	39.79	102	117.9	757.88
Input P1dB (dBm)	none	none	none	none	12	22	21	6
FOM	none	none	none	none	none	none	47.3%	66.7%
Chip area without pads	none	none	none	none	none	none	none	0.22 mm^2

Equation (7) can be rearranged as

$$V_{o3} = k(V_{i1} - V_{o2}) + V_{o1} \tag{8}$$

Equations (4), (6), and (8) can realize a VM multifunction biquadratic filter structure, which consists of a non-inverting lossless integrator, an inverting lossless integrator and a proportional gain block, as shown in Fig. 1.

Referring to (4), (6), and (7), the matrix equation of Fig. 1 can be rearranged as

$$\begin{bmatrix} 1 & \frac{1}{s\tau_1} & 0 \\ 0 & 1 & -\frac{1}{s\tau_2} \\ -1 & k & 1 \end{bmatrix} \begin{bmatrix} V_{o1} \\ V_{o2} \\ V_{o3} \end{bmatrix} = \begin{bmatrix} 0 \\ 0 \\ kV_{i1} \end{bmatrix} \tag{9}$$

According to (9), the biquadratic ILPF and BPF transfer functions at different nodes can be obtained, respectively.

$$\frac{V_{o1}}{V_{i1}} = \frac{-(\frac{k}{\tau_1\tau_2})}{s^2 + s\frac{k}{\tau_2} + \frac{1}{\tau_1\tau_2}} \tag{10}$$

$$\frac{V_{o2}}{V_{i1}} = \frac{s\frac{k}{\tau_2}}{s^2 + s\frac{k}{\tau_2} + \frac{1}{\tau_1\tau_2}} \tag{11}$$

In summary, the first proposed synthesis method has decomposed the transfer function (1) into the other two transfer functions (10) and (11). As indicated in the (1), (10) and (11), a HPF was obtained from V_{o3}, a BPF was obtained from V_{o2} and a ILPF was obtained from V_{o1}. Thus, the first block diagram based on two-integrator loop VM multifunction biquadratic filter realizes HPF, BPF and ILPF transfer functions simultaneously.

B. VM BIQUADRATIC BPF TRANSFER FUNCTION FOR ANALYSIS AND SYNTHESIS OF SYSTEM STRUCTURE

The VM transfer function of a biquadratic BPF can be given by

$$\frac{V_{o3}}{V_{i2}} = \frac{s\frac{1}{\tau_1}}{s^2 + s\frac{k}{\tau_2} + \frac{1}{\tau_1\tau_2}} \tag{12}$$

where V_{i2} is the second input signal.

Equation (12) can be simplified as follows:

$$(1 + \frac{k}{s\tau_2} + \frac{1}{s^2\tau_1\tau_2})V_{o3} = \frac{1}{s\tau_1}V_{i2} \tag{13}$$

Equation (13) can be equivalent to

$$V_{o3} = \frac{1}{s\tau_1}V_{i2} - \frac{k}{s\tau_2}V_{o3} - \frac{1}{s^2\tau_1\tau_2}V_{o3} \tag{14}$$

Equation (14) can be rearranged as

$$V_{o3} = -\frac{1}{s\tau_1}(\frac{1}{s\tau_2}V_{o3} - V_{i2}) - \frac{k}{s\tau_2}V_{o3} \tag{15}$$

Let

$$V_{o2} = \frac{1}{s\tau_2}V_{o3} \tag{16}$$

Equation (15) is then simplified as

$$V_{o3} = -\frac{1}{s\tau_1}(V_{o2} - V_{i2}) - kV_{o2} \tag{17}$$

Let

$$V_{o1} = -\frac{1}{s\tau_1}(V_{o2} - V_{i2}) \tag{18}$$

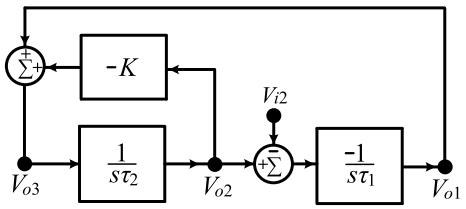

FIGURE 2. The second block diagram based on two-integrator loop VM multifunction biquadratic filter.

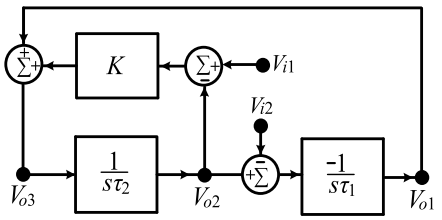

FIGURE 3. The combinations of Figs. 1 and 2 based on the superposition theorem.

Equation (17) can be simplified again as

$$V_{o3} = V_{o1} - kV_{o2} \tag{19}$$

Equations (16), (18), and (19) can realize another VM multifunction biquadratic filter structure, which consists of a non-inverting lossless integrator, an inverting lossless integrator and a proportional gain block, as shown in Fig. 2.

Referring to (16), (18) and (19), the matrix equation of Fig. 2 can be rearranged as:

$$\begin{bmatrix} 1 & \frac{1}{s\tau_1} & 0 \\ 0 & 1 & -\frac{1}{s\tau_2} \\ -1 & k & 1 \end{bmatrix} \begin{bmatrix} V_{o1} \\ V_{o2} \\ V_{o3} \end{bmatrix} = \begin{bmatrix} \frac{1}{s\tau_1} V_{i2} \\ 0 \\ 0 \end{bmatrix} \tag{20}$$

According to (20), a biquadratic LPF can be obtained at V_{o2} output terminal.

$$\frac{V_{o2}}{V_{i2}} = \frac{\frac{1}{\tau_1\tau_2}}{s^2 + s\frac{k}{\tau_2} + \frac{1}{\tau_1\tau_2}} \tag{21}$$

In summary, the second proposed synthesis method has decomposed the transfer function (12) into another transfer function (21). As indicated by (12) and (21), a biquadratic BPF function was obtained from V_{o3}, and a biquadratic LPF function was obtained from V_{o2}. Thus, the second block diagram based on two-integrator loop voltage-mode biquadratic filter realizes BPF and LPF transfer functions simultaneously.

By applying the statement superposition theorem to the combination of (9) and (20), the matrix equation can be rearranged as

$$\begin{bmatrix} 1 & \frac{1}{s\tau_1} & 0 \\ 0 & 1 & -\frac{1}{s\tau_2} \\ -1 & k & 1 \end{bmatrix} \begin{bmatrix} V_{o1} \\ V_{o2} \\ V_{o3} \end{bmatrix} = \begin{bmatrix} \frac{1}{s\tau_1} V_{i2} \\ 0 \\ kV_{i1} \end{bmatrix} \tag{22}$$

Thus, the block diagrams of Figs. 1 and 2 will be combined into a new system block as shown in Fig. 3.

C. VM CFOA-BASED BIQUADRATIC FILTER STRUCTURE REALIZATION

CFOA active components have been recognized by circuit design researchers and have drawn great attention in realizing filters and oscillators. Assuming ideal conditions, the input-output relationship of a CFOA is described by $I_Y = 0$, $V_X = V_Y$, $I_Z = I_X$ and $V_O = V_Z$ [45]. The block diagram of Fig. 3 is realized by the CFOA-based topology shown in Fig. 4. The matrix form of (22) can be used to implement a VM biquadratic filter that has two inputs and three outputs and uses three CFOAs as active elements, two grounded capacitors and four resistors. The CFOA can be commercially available and the IC AD844AN is available from Analog Devices. CFOA has several advantages, such as constant bandwidth independent of closed-loop gain, higher slew rate capability, lower sensitivity, greater dynamic range and lower power dissipation compared with traditional VM operational amplifier [27]. Moreover, CFOA has a low-output impedance, which makes the circuit to be cascaded without the need for additional buffers.

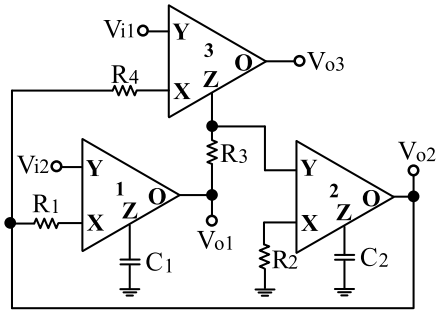

FIGURE 4. VM CFOA-based biquadratic filter configuration based on two-integrator loop structure of Fig. 3.

Based on Fig. 4, by setting $V_{i1} = V_{in}$ as input signal and leaving V_{i2} as ground zero in Fig. 4, the biquadratic ILPF, BPF and HPF transfer functions are obtained by

$$\frac{V_{o1}}{V_{in}} = \frac{-(\frac{R_3}{R_4})(\frac{1}{C_1C_2R_1R_2})}{s^2 + s\frac{R_3}{C_2R_2R_4} + \frac{1}{C_1C_2R_1R_2}} = \frac{-(\frac{k}{\tau_1\tau_2})}{s^2 + s\frac{k}{\tau_2} + \frac{1}{\tau_1\tau_2}} \tag{23}$$

$$\frac{V_{o2}}{V_{in}} = \frac{s\frac{R_3}{C_2R_2R_4}}{s^2 + s\frac{R_3}{C_2R_2R_4} + \frac{1}{C_1C_2R_1R_2}} = \frac{s\frac{k}{\tau_2}}{s^2 + s\frac{k}{\tau_2} + \frac{1}{\tau_1\tau_2}} \tag{24}$$

$$\frac{V_{o3}}{V_{in}} = \frac{(\frac{R_3}{R_4})s^2}{s^2 + s\frac{R_3}{C_2R_2R_4} + \frac{1}{C_1C_2R_1R_2}} = \frac{ks^2}{s^2 + s\frac{k}{\tau_2} + \frac{1}{\tau_1\tau_2}} \tag{25}$$

where $\tau_1 = R_1C_1$, $\tau_2 = R_2C_2$ and $k = \frac{R_3}{R_4}$.

Equations (23) to (25) show that the matrix equation of (22) can be achieved employing three CFOAs, two grounded capacitors and four resistors, thereby obtaining a new VM multifunction biquadratic filter.

By setting $V_{i2} = V_{in}$ as input signal and leaving V_{i1} as ground zero in Fig. 4, the LPF and BPF transfer functions can be obtained from the two voltage outputs V_{o2} and V_{o3} as follows.

$$\frac{V_{o2}}{V_{in}} = \frac{\frac{1}{C_1C_2R_1R_2}}{s^2+s\frac{R_3}{C_2R_2R_4}+\frac{1}{C_1C_2R_1R_2}} = \frac{\frac{1}{\tau_1\tau_2}}{s^2+s\frac{k}{\tau_2}+\frac{1}{\tau_1\tau_2}} \tag{26}$$

$$\frac{V_{o3}}{V_{in}} = \frac{s\frac{1}{C_1R_1}}{s^2+s\frac{R_3}{C_2R_2R_4}+\frac{1}{C_1C_2R_1R_2}} = \frac{s\frac{1}{\tau_1}}{s^2+s\frac{k}{\tau_2}+\frac{1}{\tau_1\tau_2}} \tag{27}$$

The control factors for the filter parameters ω_o and Q can be obtained from the denominator polynomial of the transfer functions as follows:

$$\omega_o = \sqrt{\frac{1}{C_1C_2R_1R_2}} = \sqrt{\frac{1}{\tau_1\tau_2}} \tag{28}$$

$$Q = \frac{R_4}{R_3}\sqrt{\frac{C_2R_2}{C_1R_1}} = k\sqrt{\frac{\tau_2}{\tau_1}} \tag{29}$$

According to (28) and (29), techniques for obtaining independent control of filter parameters ω_o and Q can be suggested as follows. The filter parameter Q can be independently adjusted without disturbing ω_o by changing R_3 and/or R_4. For fixed-value capacitors, the filter parameter ω_o can be independently adjusted without disturbing Q by changing R_1 and R_2 simultaneously while keeping the ratio of R_2/R_1 constant. Thus, the circuit has independent tuning capability for the filter parameters Q and ω_o.

D. INFLUENCE OF CFOA PARASITIC ELEMENTS OF THE CFOA-BASED BIQUADRATIC FILTER STRUCTURE

For an evaluation of the non-ideal performance of Fig. 4, for kth CFOA, k = 1–3, X port has a finite input resistance R_{Xk}, the parasitic components R_{Yk} connects with $1/sC_{Yk}$ in parallel at the Y port, and the parasitic components R_{Zk} connects with $1/sC_{Zk}$ in parallel at the Z port [37]. Since a resistance is connected to the X terminal of the CFOA, the parasitic resistance at X terminal of CFOA can be regarded as a part of the main resistance. Since the Z terminal of CFOA is connected to a grounded capacitor, the parasitic capacitance at Z terminal of CFOA can be regarded as a part of the main capacitance. According to Fig. 4, the parasitic resistances R_{X1}, R_{X2} and R_{X4} can be regarded as a part of the external resistances R_1, R_2 and R_4, respectively. The parasitic capacitances C_{Z1} and C_{Z2} can be absorbed into the external capacitances C_1 and C_2, respectively. The only parasitic elements that affect the circuit operation are R_{Z1}, R_{Z2}, R_{Z3}, R_{Y2}, C_{Y2} and C_{Z3}. In order to reduce the effects of parasitic impedance, the values of the external capacitors should be restricted to (30), (31) and (32).

$$\frac{1}{s(C_1+C_{Z1})} \ll R_{Z1} \tag{30}$$

$$\frac{1}{s(C_2+C_{Z2})} \ll R_{Z2} \tag{31}$$

$$R_3 \ll (R_{Y2}//R_{Z3}//\frac{1}{s(C_{Y3}+C_{Z3})}) \tag{32}$$

E. MODIFICATION OF PROPOSED CFOA-BASED FILTER AS QUADRATURE OSCILLATOR

Based on the VM BPF transfer function shown in (12), one way to obtain a quadrature sinusoidal oscillator from the transfer function is to connect the V_{o3} output signal of the filter to the V_{i2} input signal. According to the feedback theory and the Barkhausen criterion [48], [49], a biquadratic VM BPF transfer function in (12) of the loop transmission for $V_{o3} = V_{i2}$ connection is

$$\frac{s\frac{1}{\tau_1}}{s^2+s\frac{k}{\tau_2}+\frac{1}{\tau_1\tau_2}} = 1 \tag{33}$$

Based on (33), the characteristic equation of the proposed quadrature oscillator is expressed as

$$s^2 + s(\frac{k}{\tau_2} - \frac{1}{\tau_1}) + \frac{1}{\tau_1\tau_2} = 0 \tag{34}$$

In the design of the quadrature oscillator after applying Barkhausen's principle, from the real and imaginary parts of the complex number solution, the condition of oscillation (CO) and the frequency of oscillation (FO) are given by (35) and (36), respectively.

$$\text{CO:} \quad \frac{k}{\tau_2} \le \frac{1}{\tau_1} \tag{35}$$

$$\text{FO:} \quad \omega_o = \sqrt{\frac{1}{\tau_1\tau_2}} \tag{36}$$

Equations (35) and (36) prove that the biquadratic filter of Fig. 4 can be converted into a VM quadrature oscillator by making the input signal V_{i1} to ground and connecting the third CFOA Z terminal of the filter to the V_{i2} input terminal. Thus, a VM quadrature oscillator circuit is further realized in Fig. 5. By routine analysis of the circuit in Fig. 5, the equation of the quadrature oscillator characteristic is expressed as

$$s^2 + s(\frac{R_3}{C_2R_2R_4} - \frac{1}{C_1R_1}) + \frac{1}{C_1C_2R_1R_2} = s^2 + s(\frac{k}{\tau_2} - \frac{1}{\tau_1}) + \frac{1}{\tau_1\tau_2} = 0 \tag{37}$$

where $\tau_1 = R_1C_1$, $\tau_2 = R_2C_2$ and $k = \frac{R_3}{R_4}$.

Hence, the CO and FO of the proposed VM quadrature oscillator in Fig. 5 can be expressed as follows:

$$\text{CO:} \quad \frac{R_3}{C_2R_2R_4} \le \frac{1}{C_1R_1} \tag{38}$$

$$\text{FO:} \quad \omega_o = \sqrt{\frac{1}{C_1C_2R_1R_2}} \tag{39}$$

According to (38) and (39), the following techniques can be proposed to obtain independent control of parameters CO and FO. Taking $C_1 = C_2 = C$ and $R_1 = R_2 = R$, the recommended design equations for the specified CO and FO are as follows:

$$\text{CO:} \quad R_3 \le R_4 \tag{40}$$

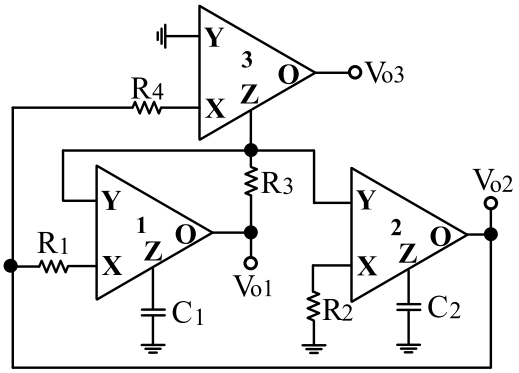

FIGURE 5. Proposed VM quadrature sinusoidal oscillator based on modification the filter of Fig. 4.

$$\text{FO}: \quad \omega_o = \frac{1}{CR} \tag{41}$$

Based on (40) and (41), the CO can be independently controlled without disturbing FO by adjusting R_3 and/or R_4. The FO can be controlled without disturbing CO by adjusting R. Thus, the VM quadrature oscillator enjoys the advantage of independent control of CO and FO.

The VM quadrature oscillator output voltages V_{o2} and V_{o3} of Fig. 5 are as

$$V_{o2} = \frac{1}{sC_2R_2} V_{o3} \tag{42}$$

The relationship between the two voltage outputs in the steady state are as

$$V_{o2} = \frac{1}{\omega_o C_2 R_2} e^{-j\varphi} V_{o3} \tag{43}$$

where the phase difference is ensure that the voltages V_{o2} and V_{o3} are quadrature, $\varphi = 90°$. Restated, the filter can be converted into a VM quadrature oscillator, and two quadrature voltage outputs can be proven by modifying one connection appropriately.

III. SIMULATION AND EXPERIMENTAL RESULTS

A. PROPOSED AD844-TYPE CFOA-BASED FILTER

To prove the performances of the proposed circuits, PSpice simulations were used for examination and experimentation. For the simulations, the proposed filter was constructed from the built-in library AD844/AD. For the experiments, the proposed filter was constructed in the laboratory using commercially available AD844AN ICs. The supply voltage of simulated and experimental results were ±6 V. To obtain a pole frequency of $f_o = 117.9$ kHz at $Q = 1$, set the component values to $R_1 = R_2 = R_3 = R_4 = 3$ kΩ and $C_1 = C_2 = 450$ pF. Figures 6 to 8 represent the simulated and measured frequency responses of ILPF (V_{o1}), BPF (V_{o2}) and HPF (V_{o3}) by choosing $V_{i1} = V_{in}$ and $V_{i2} = 0$, respectively. Figures 9 and 10 represent the simulated and measured frequency responses of LPF (V_{o2}) and BPF (V_{o3}) by choosing $V_{i1} = 0$ and $V_{i2} = V_{in}$, respectively. The power consumption of the simulation and measurement

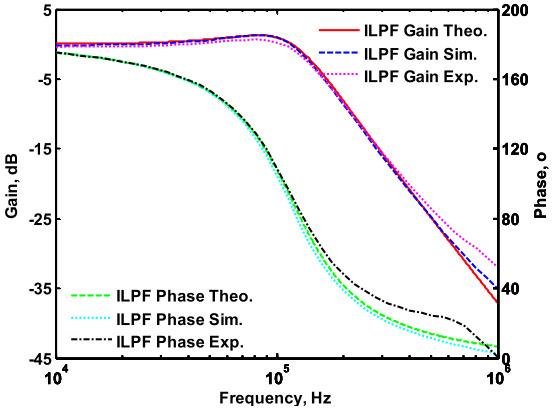

FIGURE 6. Simulated and experimental ILPF with the theory responses.

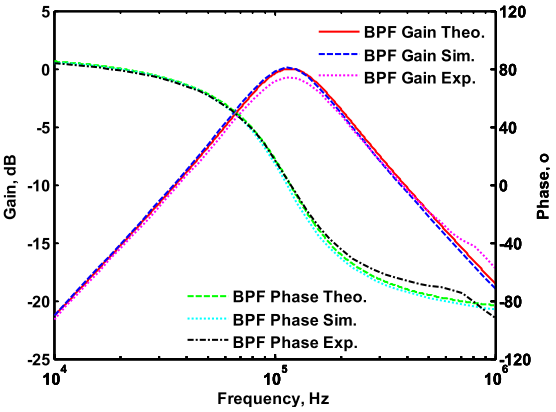

FIGURE 7. Simulated and experimental BPF with the theory responses.

results are approximately 255 mW and 168 mW, respectively. Figures 11 and 12 show that the filter parameters Q and f_o can be specified recommended independently controllable, respectively. In Fig. 11, the Q changes (0.67, 1 and 1.67) when f_o is maintained at 117.9 kHz. The component values used in Fig. 11 are $R_1 = R_2 = R_3 = 3$ kΩ, $C_1 = C_2 = 450$ pF, and change resistor $R_4 = 2$, 3 and 5 kΩ, resulting in $Q = 0.67$, 1 and 1.67, respectively. For fixed-value capacitors, Fig. 12 shows the parameter f_o was tuned without disturbing Q by simultaneously changing R_1 and R_2 while keeping the ratio of R_2/R_1 constant. In Fig. 12, the parameter f_o varies (176.8, 117.9 and 88.4 kHz) when Q remains at 1. The component values used in Fig. 12 remain $C_1 = C_2 = 450$ pF, $R_3 = R_4 = 3$ kΩ, while changing $R_1 = R_2$ at different values of 2, 3 and 4 kΩ, resulting in $f_o = 176.8$, 117.9 and 88.4 kHz, respectively. In Figs. 6 to 12, the simulation and measurement results were found to be consistent with theoretical analysis. However, the non-ideal characteristics, parasitic resistances and capacitances of the AD844AN ICs, the printed circuit board layout issue, and the tolerances of the working resistors and capacitors will have effects on circuit accuracy.

Regarding the input dynamic range of the AD844-type CFOA-based biquadratic filter, the passive component values

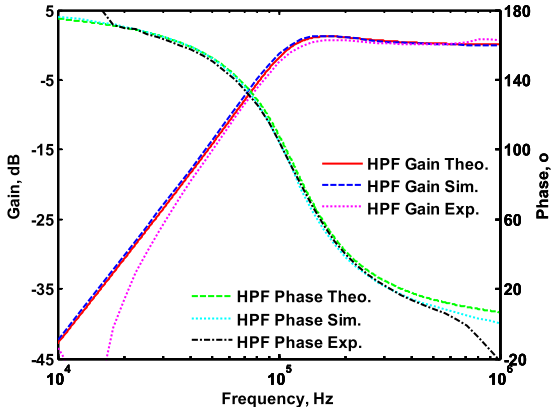

FIGURE 8. Simulated and experimental HPF with the theory responses.

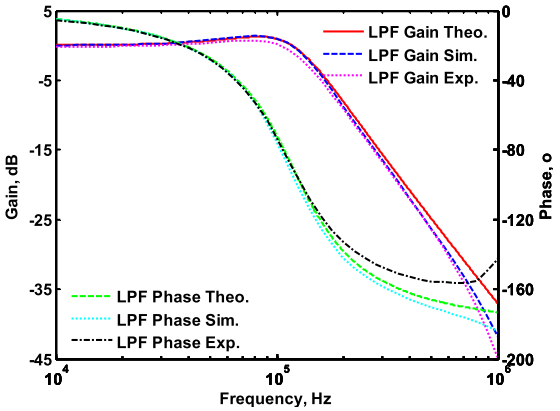

FIGURE 9. Simulated and experimental LPF with the theory responses.

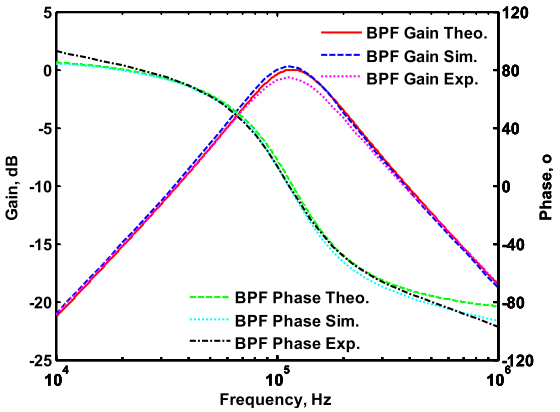

FIGURE 10. Simulated and experimental BPF with the theory responses.

were chosen as $R_i = 3$ kΩ ($i = 1$ to 4), $C_1 = C_2 = 450$ pF, and the center frequency of $f_o = 117.9$ kHz can be obtained. The time-domain BPF response of the proposed AD844-type filter was investigated by applying a 5.68 V_{pp} (peak-to-peak) sinusoidal input voltage at a frequency of 117.9 kHz. Figure 13 shows the measured BPF output response waveform at the V_{o3} output terminal when $V_{i1} = 0$ and $V_{i2} = V_{in}$. The dynamic range is expended to an amplitude of 5.68 V_{pp}, resulting in a phase shift of approximately 5.3-degrees. The

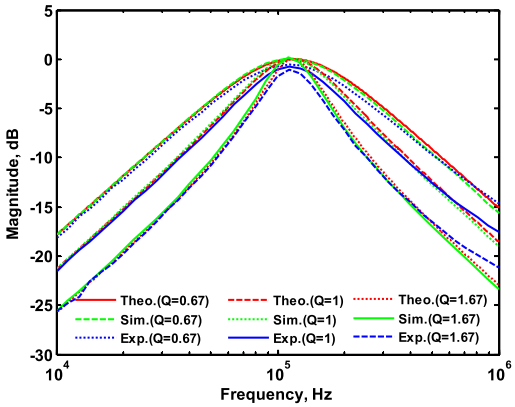

FIGURE 11. Gain responses of the BPF (V_{o2}) by varying Q while keeping f_o when $V_{i1} = V_{in}$ and $V_{i2} = 0$.

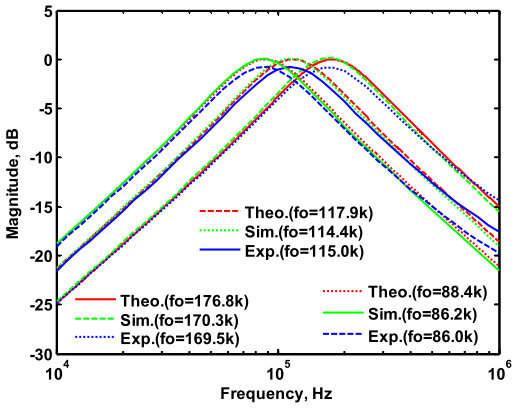

FIGURE 12. Gain responses of the BPF (V_{o2}) by varying f_o while keeping Q when $V_{i1} = V_{in}$ and $V_{i2} = 0$.

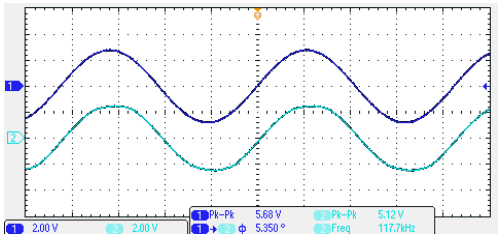

FIGURE 13. The input (channel 1, blue line) and output (channel 2, cyan line) time-domain experimental waveforms of BPF.

following FOM is shown in (44), which is based on the ratio of the input voltage to power supply voltage, V_{in} / V_{dd} [2]. Based on (44), the FOM of AD844-type filter is 47.3%. Figure 14 shows the measured output spectrum of Fig. 13. The dependence of the output harmonic distortion on the input voltage amplitude is illustrated in Fig. 15.

$$\text{FOM} = 100 \times (V_{in}/V_{dd})\% \tag{44}$$

The linearity of the proposed AD844-type biquadratic filter is evaluated by examining the 1-dB power gain compression point, P1dB. To represent the linearity of the proposed filter, the P1dB is the measured value of the BPF output

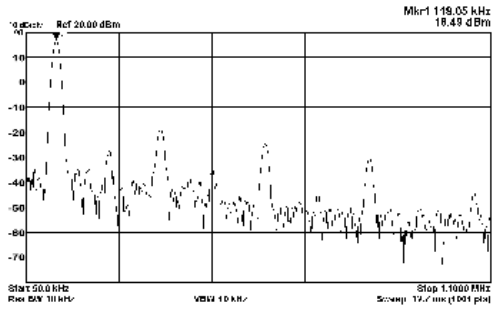

FIGURE 14. The experimental AD844-type BPF frequency spectrum of Fig. 13.

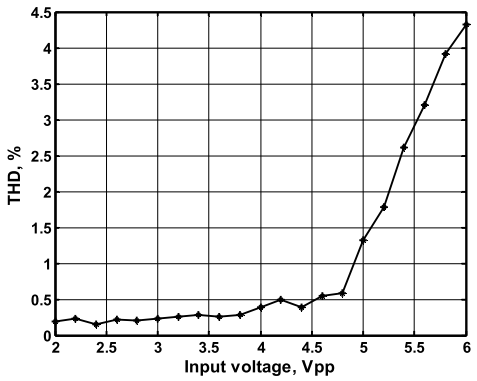

FIGURE 15. The THD measurement analysis results of AD844-type BPF at V_{o3} output terminal with input voltage signal at 117.9 kHz.

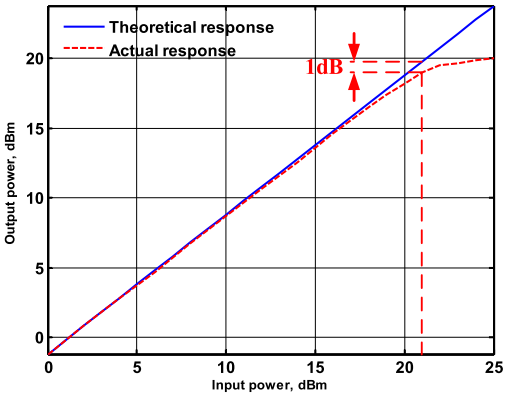

FIGURE 16. The P1dB measurement of the AD844-type BPF with input power.

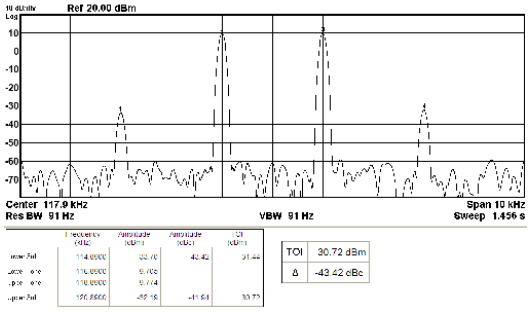

FIGURE 17. The AD844-type BPF output spectrum for a two-tone intermodulation distortion test.

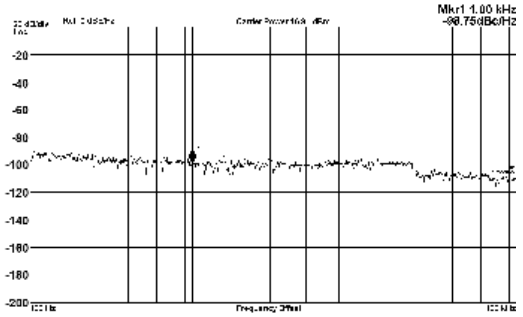

FIGURE 18. The phase noise measurement of the proposed AD844-type BPF.

voltage V_{o3} with $V_{i1} = 0$ and $V_{i2} = V_{in}$ by applying the input power at the center frequency of 117.9 kHz. The measured value of the input P1dB is about 21 dBm, and the AD844-type biquadratic filter input/output (I/O) power curve is shown in Fig. 16. To represent the nonlinearity of proposed filter in Fig. 4, a two-tone intermodulation distortion (IMD) test has been used to characterize the nonlinearity of BPF response at V_{o3} output terminal when $V_{i1} = 0$ and $V_{i2} = V_{in}$. Selecting $R_i = 3$ kΩ ($i = 1$ to 4) and $C_1 = C_2 = 450$ pF results in an angular frequency of $f_o = 117.9$ kHz. Figure 17 shows the BPF response spectrum described through intermodulation characterization by applying two-tone signals, f_1 and f_2, near the angular frequency of $f_o = 117.9$ kHz. In Fig. 17, a low-frequency tone at $f_1 = 116.89$ kHz and a high-frequency tone at $f_2 = 118.89$ kHz are used, and the input amplitude is 4.6 V_{pp}. As shown in Fig. 17, the measured value of the third-order intermodulation distortion (IMD3) is around −43.42 dBc and the third-order intercept (TOI) point is around 30.72 dBm. Figure 18 shows the phase noise performance of the proposed filter using the Agilent phase noise measurement. In Fig. 18, the phase noise of measured input of the BPF on the V_{o3} output terminal when $V_{i1} = 0$ and $V_{i2} = V_{in}$, where 5.68 V_{pp} sinusoidal input voltage at 117.9 kHz is applied to the AD844-type biquadratic filter. The measure phase noise of the AD844-type biquadratic filter is less than −98.75 dBc/Hz at 1 kHz offset.

B. PROPOSED AD844-TYPE CFOA-BASED QUADRATURE OSCILLATOR

To obtain the sinusoidal output waveform with the theoretical oscillation frequency of $f_o = 117.9$ kHz, the component values used in Fig. 5 were chosen as $C_1 = C_2 = 450$ pF, $R_1 = R_2 = R_4 = 3$ kΩ and $R_3 = 2.95$ kΩ. Figure 19 shows the measurement of quadrature sinusoidal waveforms. The result confirms the function of the quadrature sinusoidal waveforms and shows that the measured oscillation frequency is 118.2 kHz and the phase difference between the two output waveforms is 86.1 degrees. The output spectrum, V_{o3}, of the proposed oscillator is shown in Fig. 20. The verification result is that the measured oscillation frequency (117.5 kHz) is close

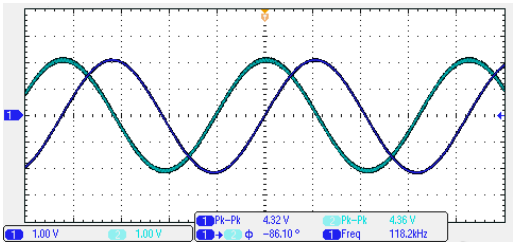

FIGURE 19. The measurement of the quadrature voltage outputs V_{o2} (blue) and V_{o3} (cyan) in Fig. 5.

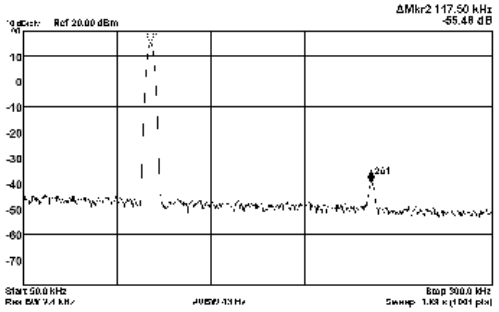

FIGURE 20. The experimental frequency spectrum of V_{o3}.

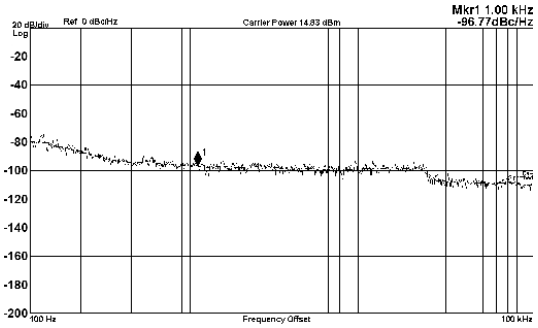

FIGURE 21. The phase noise measurement of the proposed AD844-type oscillator.

to the theoretical value (117.9 kHz). Moreover, the second harmonic noise power is 55.48 dB lower than the fundamental harmonic signal power, and the THD of the proposed oscillator is about 0.17%. Figure 21 shows the phase noise performance of the proposed oscillator. The measured results show that the phase noise is less than −96.77 dBc/Hz at a 1 kHz offset.

C. IMPLEMENTATION AND MEASUREMENT OF CFOA-BASED FILTER AND OSCILLAOTR IC

The filter presented in Fig. 4 and Section III-A have been verified through PSpice simulations and hardware implementations based on AD844-type CFOAs and ±6 V DC power supplies. Because the circuit is implemented in Section III-A using commercial AD844-type CFOAs and discrete passive components on the breadboard, the highest applicable operating frequency of the proposed filter only demonstrates tens of kilohertz to megahertz, as shown in Figs. 6 to 12. In addition,

TABLE 2. Aspect ratio of the MOS transistors in the proposed CFOA.

Transistors	L (μm)	W (μm)
M1, M2, M17, M18	0.8	13
M3 - M6, M19 - M22	0.4	26
M7 - M16, M23 - M28	0.4	75

the power consumption of the AD844-type filter is high and the FOM of AD844-type filter is 47.3%. To overcome this problem, high-speed, low-power consumption and the highest FOM value of CMOS CFOA components can be used to increase the operating frequency, thereby decreasing power consumption and increasing the FOM value. Therefore, the proposed IC based on CFOA filter and oscillator is implemented in the chip by adapting TSMC 0.18 μm level-49 1P6M CMOS process. Figure 22 shows the chip photograph and layout of the proposed CFOA-based filter and oscillator. In Fig. 22, the passive components used in the filter design are chosen as $C_1 = C_2 = 15$ pF and $R_1 = R_2 = R_3 = R_4 = 14$ kΩ. The passive components used in the oscillator design in Fig. 22 are chosen as $C_1 = C_2 = 15$ pF, $R_1 = R_2 = R_3 = 14$ kΩ and $R_4 = 14.4$ kΩ. In chip fabrication, polysilicon is used for passive components of resistors, and metal-insulator-metal (MIM) is used for capacitors. The CFOAs of the chip developed in Fig. 22 is based on the novel CMOS structure illustrated in Fig. 23. The aspect ratio of MOS transistors in Fig. 23 is given in Table 2. In Fig. 22, the center frequency of the proposed chip is designed as $f_o = 757.88$ kHz for the CFOA-based filter and oscillator IC. The supply voltages are $V_{DD} = -V_{SS} = 0.9$ V, and the biasing voltages are $V_{B1} = 0.6$ V and $V_{B2} = 0.3$ V. The total power dissipation of the filter/oscillator chip cell is approximately 5.4 mW. The chip area without pads of the filter/oscillator cell is 0.22 mm^2. To verify the effectiveness of the CFOA-based filter chip cell, the on-chip function of the proposed filter chip cell has been verified by the measurement results of the network spectrum. Figures 24 to 26 represent the chip frequency responses of ILPF (V_{o1}), BPF (V_{o2}) and HPF (V_{o3}) by choosing $V_{i1} = V_{in}$ and $V_{i2} = 0$, respectively. Figures 27 and 28 represent the chip frequency responses of LPF (V_{o2}) and BPF (V_{o3}) by choosing $V_{i1} = 0$ and $V_{i2} = V_{in}$, respectively. As shown in Figs. 24 to 28, the experimental results are close to the theoretical values. Moreover, when the supply voltage changes from ± 0.8 V to ± 1 V, the measured BPF center frequency changes from 782.6 kHz to 735.9 kHz, which affect the center frequency in a range of +3.26% to −2.9%, respectively. The simulation results show that when the temperature changes from 0° to 80°, the BPF center frequency changes from 714.1 kHz to 816.8 kHz, which affect the center frequency in a range of −5.78% to +7.77%, respectively.

Regarding the input dynamic range of the CFOA-based filter chip cell was also investigated. Figure 29 shows the input dynamic range of the BPF measured on the V_{o3} output terminal when $V_{i1} = 0$ and $V_{i2} = V_{in}$, where a 1.2 V_{pp} sinusoidal input voltage at 757.88 kHz is applied to the

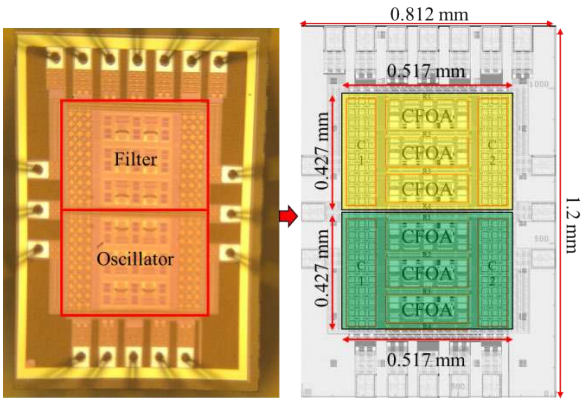

FIGURE 22. Chip photograph and layout of the proposed CFOA-based filter and oscillator.

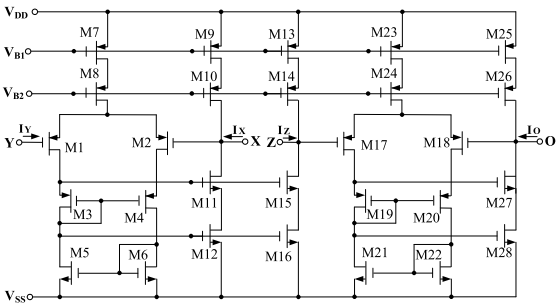

FIGURE 23. CMOS realization of the CFOA.

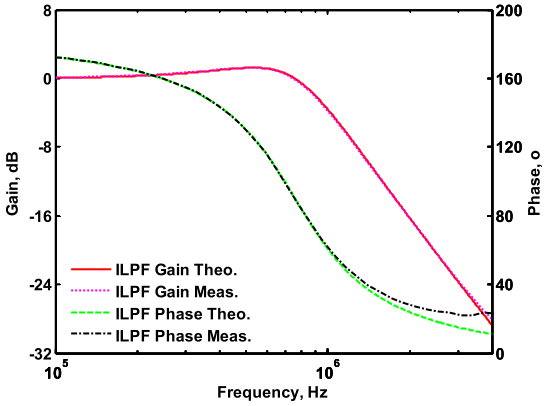

FIGURE 24. The magnitude and phase response measurements of ILPF based on the filter chip cell at V_{o1} output terminal.

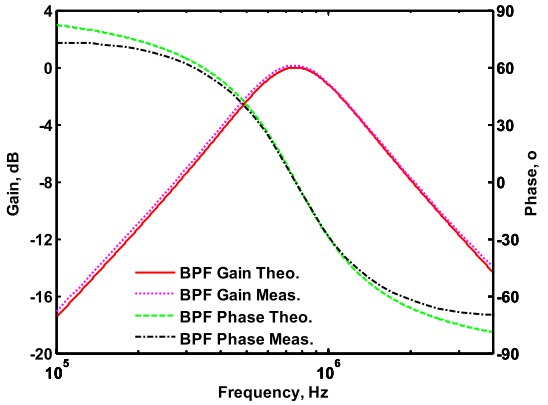

FIGURE 25. The magnitude and phase response measurements of BPF based on the filter chip cell at V_{o2} output terminal.

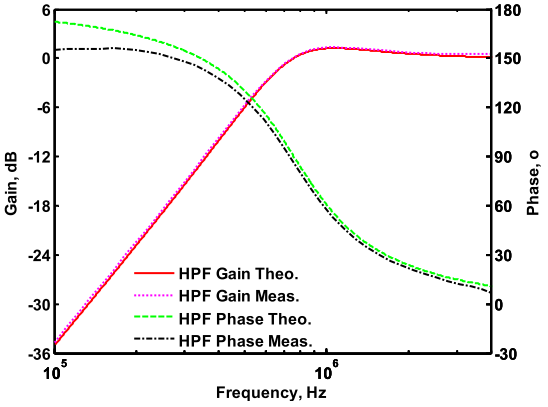

FIGURE 26. The magnitude and phase response measurements of HPF based on the filter chip cell at V_{o3} output terminal.

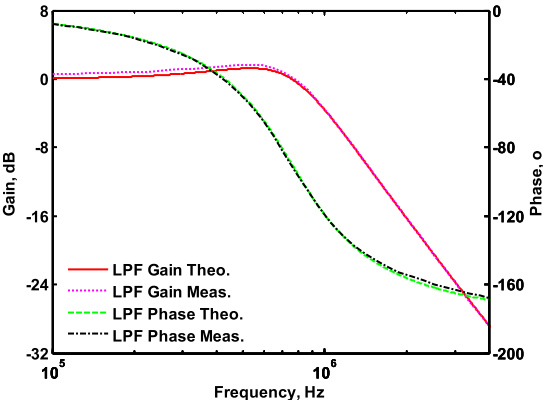

FIGURE 27. The magnitude and phase response measurements of LPF based on the filter chip cell at V_{o2} output terminal.

CFOA-based filter chip cell of Fig. 22. The dynamic range is extended to an amplitude of 1.2 V_{pp} without signification distortion. Based on (44), the FOM of CFOA-based filter chip cell is 66.7%. In Fig. 29, the measured angular frequency is about 757.6 kHz, which is very close to theoretical value of 757.88 kHz. Figure 30 shows the measured output spectrum of Fig. 29. As shown in Fig. 30, the THD is about 3.18%, when the input signal increases to 1.2 V_{pp} sinusoidal voltage at 757.88 kHz. Figure 31 shows the dependence of output harmonic distortion on input voltage amplitude.

To represent the linearity of the proposed CFOA-based filter chip cell, the P1dB is the measured value of the BPF output voltage V_{o3}, which is obtained by applying the input power at the center frequency of 757.88 kHz when $V_{i1} = 0$ and $V_{i2} = V_{in}$. The measured value of the input P1dB is about 6 dBm, and the I/O power waveform of the CFOA-based filter chip cell is shown in Fig. 32. Figure 33 shows the filter's

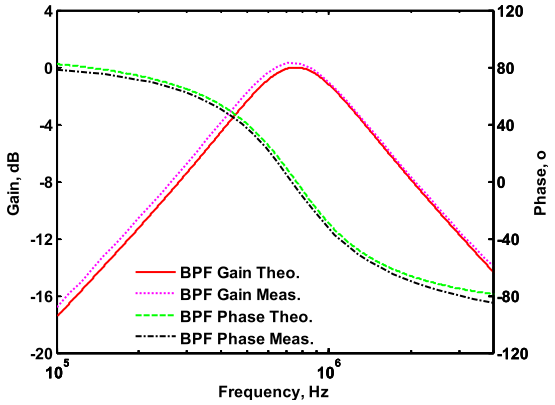

FIGURE 28. The magnitude and phase response measurements of BPF based on the filter chip cell at V_{o3} output terminal.

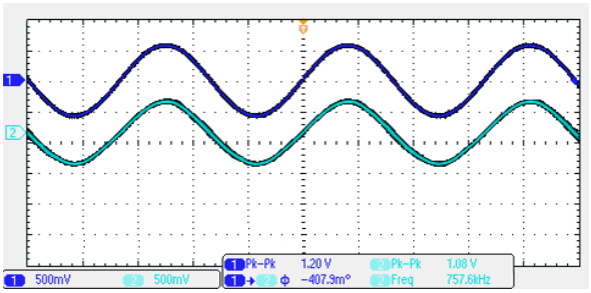

FIGURE 29. The input (channel 1, blue line) and output (channel 2, cyan line) time-domain experimental waveforms of BPF based on the filter chip cell at V_{o3} when input voltage signal at 757.88 kHz.

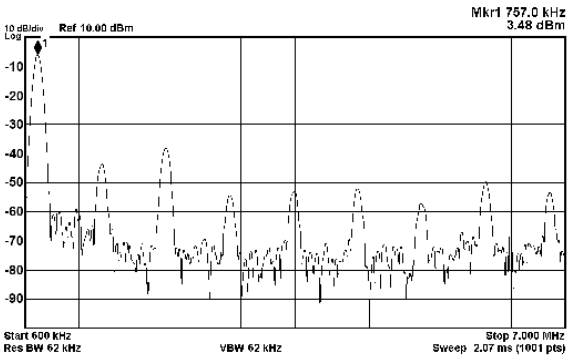

FIGURE 30. The frequency spectrum measurement of Fig. 29.

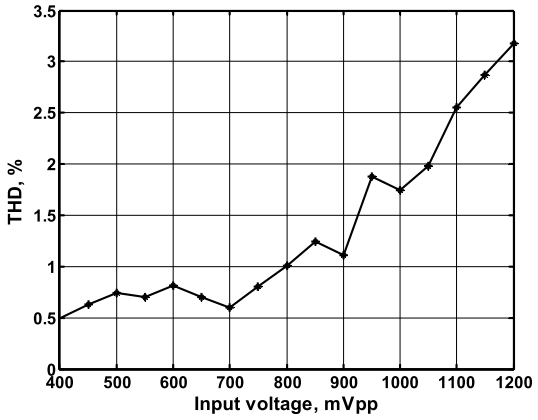

FIGURE 31. The THD measurement result of BPF based on the filter chip cell at V_{o3} output terminal.

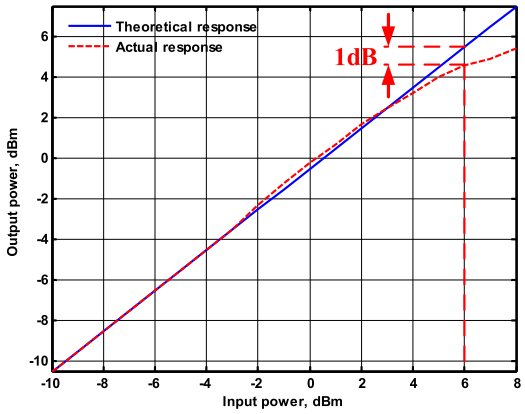

FIGURE 32. The P1dB measurement of BPF based on the filter chip cell with input power at V_{o3} output terminal.

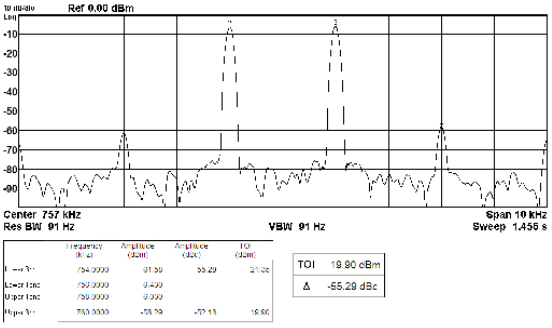

FIGURE 33. The two-tone (756 and 758 kHz) intermodulation distortion test based on the BPF filter chip cell at V_{o3} output spectrum.

output spectrum for two tones applied at 756 and 758 kHz with an amplitude of 0.7 V_{pp} each. As shown in Fig. 33, the measured value of the IMD3 is around −55.29 dBc and the TOI point is around 19.9 dBm. Figure 34 shows the phase noise of the BPF measured on the V_{o3} output terminal when $V_{i1} = 0$ and $V_{i2} = V_{in}$, where a 1.2 V_{pp} sinusoidal input voltage of 757.88 kHz is applied to the CFOA-based filter chip cell. The measured phase noise of the CFOA-based filter chip cell is less than −99.76 dBc/Hz at 1 kHz offset.

Consequently, Table 3 summarizes two technical verification methods for the proposed filter specifications with commercial AD844-type ICs and CMOS CFOA-based filter chip cell. As Table 3 indicates, the proposed CFOA-based filter chip cell has low power consumption, the highest FOM value and a small core area, which makes its performance better than the filter implemented by AD844-type IC and is suitable for system-on-chip applications.

The paper also investigates the CFOA-based oscillator chip cell. To obtain the sinusoidal output waveform with the theoretical oscillation frequency of $f_o = 757.88$ kHz,

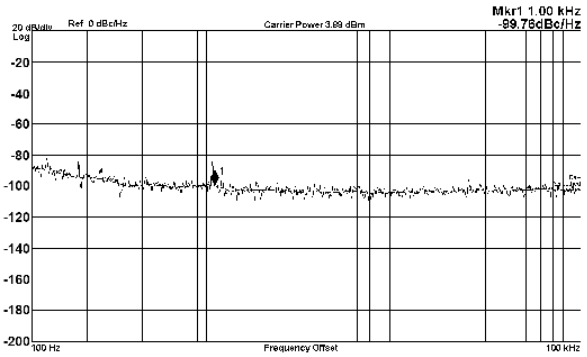

FIGURE 34. The phase noise measurement based on the BPF filter chip cell at V_{o3} output terminal.

TABLE 3. Comparison of performance specifications of the proposed filter with commercial IC and chip implemented.

Parameter	Commercial IC	Proposed CFOA-based filter chip cell
Technology	AD844	0.18μm 1P6M CMOS
Power supply	±6 V	±0.9 V
Power consumption	168 mW	5.4 mW
Chip area	none	0.22 mm^2
Center frequency	117.9 kHz	757.88 kHz
Input voltage range	5.68 V_{pp}	1.2 V_{pp}
THD	3.2% (@freq.= 117.9 kHz, V_{in} = 5.68 V_{pp})	3.18% (@freq.=757.88 kHz, V_{in} = 1.2 V_{pp})
P1dB	21 dBm	6 dBm
TOI	30.72 dBm	19.9 dBm
IMD3	−43.42 dBc	−55.29 dBc
Phase noise	−98.75 dBc/Hz (@1 kHz offset)	−99.76 dBc/Hz (@1 kHz offset)
FOM	47.3%	66.7%

the component values used in Fig. 22 are chosen as $C_1 = C_2 = 15$ pF, $R_1 = R_2 = R_3 = 14$ kΩ and $R_4 = 14.5$ kΩ. Figure 35 shows the measurement of the CFOA-based oscillator chip cell quadrature sinusoidal waveforms. The result confirms the function of the quadrature sinusoidal waveforms and shows that the measured oscillation frequency is 744.2 kHz and the phase difference between the two output waveforms is 86.2 degrees. The output spectrum, V_{o3}, of the CFOA-based oscillator chip cell is shown in Fig. 36. The verification result is that the measured oscillation frequency (746 kHz) is close to the theoretical value (757.88 kHz). Figure 37 shows the phase noise performance of the CFOA-based oscillator chip cell. The measured results show that the phase noise is less than −40.77 dBc/Hz at 1 kHz offset. The excellent performances in terms of phase-noise FOM is defined as follows [50].

$$\mathrm{FOM}(\Delta\omega) = -L(\Delta\omega) + 20\log(\frac{\omega_o}{\Delta\omega}) - 10\log(\frac{P_{DC}}{1mW}) \tag{45}$$

where $L(\Delta\omega)$ is the phase noise at the offset frequency to the carrier, $\Delta\omega$ is the offset frequency relative to the carrier, ω_o is

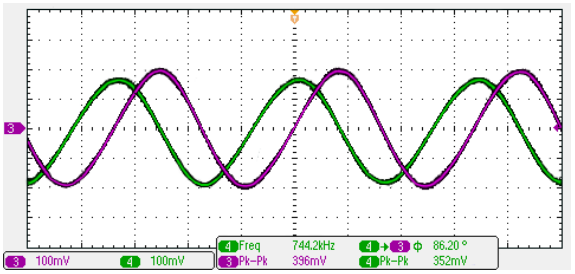

FIGURE 35. The quadrature voltage outputs V_{o2} (purple) and V_{o3} (green) measurements of the oscillator chip cell in Fig. 22.

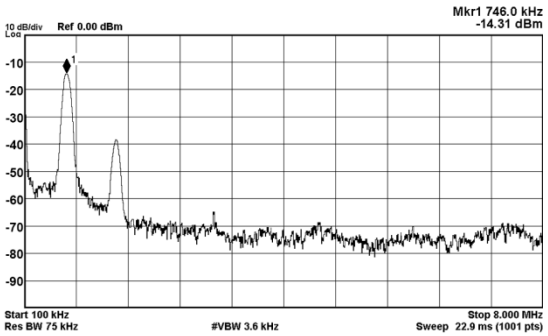

FIGURE 36. The experimental frequency spectrum of the oscillator chip cell in Fig. 22.

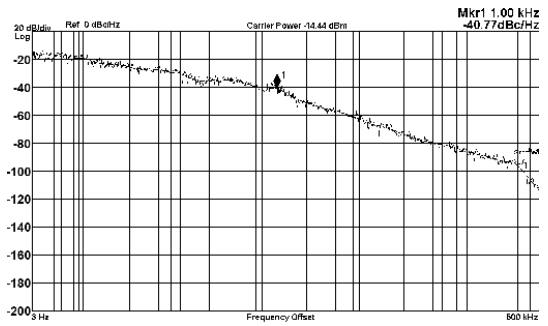

FIGURE 37. The phase noise measurement of the oscillator chip cell in Fig. 22.

the oscillation frequency, and P_{DC} is the power consumption. According to (45), the FOM of the CFOA-based oscillator chip cell is 90.9 dBc/Hz.

IV. CONCLUSION

In this paper, an approach for the systematic and structural method of two voltage lossless integrators and a voltage proportional block based on the use of CFOAs has been presented. The proposed VM biquadratic filter with two inputs and three outputs uses three CFOAs, two grounded capacitors and four resistors. The filter can simultaneously generate the VM HPF, BPF and ILPF transfer functions or the VM BPF and LPF transfer functions. The filter parameters ω_o and Q are independently controllable by adjusting the values of resistors. The filter has high-input impedance and is suitable for cascading in VM operation. By slightly modifying

the proposed filter, a VM quadrature sinusoidal oscillator is easily achieved. The CO and FO can be independently controllable. The theoretical results are confirmed by simulation and experimental results. In addition, the proposed VM biquadratic filter and oscillator were fabricated with TSMC 0.18 μm CMOS 1P6M process technology. Compared with the off-the-shelf CFOA-type AD844 ICs, the realization of the CMOS CFOA-based filter chip cell has obtained better characteristics verification. An attractive feature of CFOA-based biquadratic filter with high-input impedance is that the VM HPF, BPF and ILPF outputs or the VM BPF and LPF outputs can be implemented on-chip simultaneously. The power consumption of the filter chip cell is 5.4 mW with a power supply of $\pm$0.9 V. The core area without pads of the CFOA-based filter/oscillator chip cell is 0.22 mm^2. The measured value of the IMD3 is around $-$55.29 dBc, and the TOI point is around 19.9 dBm. The measured phase noise of the CFOA-based filter chip cell is less than $-$99.76 dBc/Hz at 1 kHz offset. The FOM of CFOA-based filter chip cell is 66.7%. The measured phase noise of the CFOA-based oscillator chip cell is less than $-$40.77 dBc/Hz at 1 kHz offset. The FOM of CFOA-based oscillator chip cell is 90.9 dBc/Hz.

REFERENCES

[1] S. Y. Tseng and R.-B. Wu, "Synthesis of chebyshev/elliptic filters using minimum acoustic wave resonators," *IEEE Access*, vol. 7, pp. 103456–103462, 2019.

[2] P.-H. Liao, Y.-S. Hwang, J.-J. Chen, Y. Ku, and S.-F. Wang, "A new low-voltage operational transconductance amplifier with push-pull CMFB scheme for low-pass filter applications," *AEU-Int. J. Electron. Commun.*, vol. 123, Aug. 2020, Art. no. 153298.

[3] S. Maheshwari, J. Mohan, and D. S. Chauhan, "Voltage-mode cascadable all-pass sections with two grounded passive components and one active element," *IET Circuits Devices Syst.*, vol. 4, no. 2, pp. 113–122, 2010.

[4] Y. S. Hwang, A. Liu, S. F. Wang, S. C. Yang, and J. J. Chen, "A tunable butterworth low-pass filter with digitally controlled DDCC," *Radioengineering*, vol. 22, no. 2, pp. 511–517, 2013.

[5] Y. S. Hwang, Y. T. Ku, J. J. Chen, and C. C. Yu, "Inverter-based low-voltage CCII-design and its filter application," *Radioengineering*, vol. 23, no. 4, pp. 1026–1033, 2013.

[6] C. Chang, S. Tu, M. N. S. Swamy, and A. M. Soliman, "Analytical synthesis of *elliptic* voltage-mode even/odd-*nth*-order filter structures using DDCCs, FDCCIIs, and grounded capacitors and resistors," *IET Circuits, Devices Syst.*, vol. 13, no. 3, pp. 279–291, May 2019.

[7] H. Chen, "High-input impedance voltage-mode differential difference current conveyor transconductance amplifier-based universal filter with single input and five outputs using only grounded passive components," *IET Circuits, Devices Syst.*, vol. 8, no. 4, pp. 280–290, Jul. 2014.

[8] J. Jin, K.-Q. Zhou, and L. Zhao, "Designing RF ring oscillator using current-mode technology," *IEEE Access*, vol. 5, pp. 5306–5312, 2017.

[9] S. Hong, S. Lee, J. Lee, and M. Je, "A multi-mode ULP receiver based on an injection-locked oscillator for IoT applications," *IEEE Access*, vol. 8, pp. 76966–76979, 2020.

[10] P. Andreani, "A time-variant analysis of the 1/f^2 phase noise in CMOS parallel LC-tank quadrature oscillators," *IEEE Trans. Circuits Syst. I, Reg. Papers Reg. Papers*, vol. 53, no. 8, pp. 1749–1760, Aug. 2006.

[11] Y.-S. Hwang, C.-M. Kung, H.-C. Lin, and J.-J. Chen, "Low-sensitivity, low-bounce, high-linearity current-controlled oscillator suitable for single-supply mixed-mode instrumentation system," *IEEE Trans. Ultrason., Ferroelectr., Freq. Control*, vol. 56, no. 2, pp. 254–262, Feb. 2009.

[12] S.-H. Tu, Y.-S. Hwang, J.-J. Chen, A. M. Soliman, and C.-M. Chang, "OTA-C arbitrary-phase-shift oscillators," *IEEE Trans. Instrum. Meas.*, vol. 61, no. 8, pp. 2305–2319, Aug. 2012.

[13] A. Nikoofard, S. Kananian, and A. Fotowat-Ahmady, "Off-resonance oscillation, phase retention, and orthogonality modeling in quadrature oscillators," *IEEE Trans. Circuits Syst. I, Reg. Papers*, vol. 63, no. 6, pp. 883–894, Jun. 2016.

[14] M. T. Abuelma'atti, A. A. Farooqi, and S. M. Alshahrani, "Novel RC oscillators using the current-feedback operational amplifier," *IEEE Trans. Circuits Syst. I, Fundam. Theory Appl.*, vol. 43, no. 2, pp. 155–157, Feb. 1996.

[15] V. K. Singh, A. K. Singh, D. R. Bhaskar, and R. Senani, "Novel mixed-mode universal biquad configuration," *IEICE Electron. Exp.*, vol. 2, no. 22, pp. 548–553, 2005.

[16] M. A. Ibrahim, S. Minaei, and H. Kuntman, "A 22.5 MHz current-mode KHN-biquad using differential voltage current conveyor and grounded passive element," *AEU Int. J. Electron. Commun.*, vol. 59, no. 5, pp. 311–318, 2005.

[17] C.-M. Chang, "Analytical synthesis of the digitally programmable voltage-mode OTA-C universal biquad," *IEEE Trans. Circuits Syst. II, Exp. Briefs*, vol. 53, no. 8, pp. 607–611, Aug. 2006.

[18] C.-M. Chang, A. M. Soliman, and M. N. S. Swamy, "Analytical synthesis of low-sensitivity high-order voltage-mode DDCC and FDCCII-grounded *R* and *C* all-pass filter structures," *IEEE Trans. Circuits Syst. I, Reg. Papers*, vol. 54, no. 7, pp. 1430–1443, Jul. 2007.

[19] W.-Y. Chiu and J.-W. Horng, "High-input and low-output impedance voltage-mode universal biquadratic filter using DDCCs," *IEEE Trans. Circuits Syst. II, Exp. Briefs*, vol. 54, no. 8, pp. 649–652, Aug. 2007.

[20] Y. S. Hwang, D. S. Wu, J. J. Chen, C. C. Shih, and W. S. Chou, "Design of current-mode MOSFET-C filters using OTRAs," *Int. J. Circuit Theory Appl.*, vol. 37, no. 3, pp. 397–411, 2009.

[21] Y.-S. Hwang, S.-H. Tu, W.-H. Liu, and J.-J. Chen, "New building block: Multiplication-mode current conveyor," *IET Circuits, Devices Syst.*, vol. 3, no. 1, pp. 41–48, Feb. 2009.

[22] S. Minaei and M. A. Ibrahim, "A mixed-mode KHN-biquad using DVCC and grounded passive elements suitable for direct cascading," *Int. J. Circuit Theory Appl.*, vol. 37, no. 7, pp. 793–810, Sep. 2009.

[23] K. K. Abdalla, D. R. Bhaskar, and R. Senani, "Configuration for realising a current-mode universal filter and dual-mode quadrature single resistor controlled oscillator," *IET Circuits Devices Syst.*, vol. 6, pp. 159–167, 2012.

[24] A. Lahiri, W. Jaikla, and M. Siripruchyanun, "First CFOA-based explicit-current-output quadrature sinusoidal oscillators using grounded capacitors," *Int. J. Electron.*, vol. 100, no. 2, pp. 259–273, Feb. 2013.

[25] H. P. Chen, S. F. Wang, Y. T. Ku, and M. Y. Hsieh, "Quadrature oscillators using two CFOAs and four passive components," *IEICE Electron. Exp.*, vol. 12, no. 2, pp. 1–8, 2015.

[26] S.-I. Liu and D.-S. Wu, "New current-feedback amplifier-based universal biquadratic filter," *IEEE Trans. Instrum. Meas.*, vol. 44, no. 4, pp. 915–917, Aug. 1995.

[27] J. W. Horng, "New configuration for realizing universal voltage-mode filter using two current feedback amplifiers," *IEEE Trans. Instrum. Meas.*, vol. 49, no. 5, pp. 1043–1045, Oct. 2000.

[28] J.-W. Horng, "Voltage-mode multifunction filter using one current feedback amplifier and one voltage follower," *Int. J. Electron.*, vol. 88, no. 2, pp. 153–157, Feb. 2001.

[29] N. A. Shah, M. F. Rather, and S. Z. Iqbal, "CFA-based three input and two outputs voltage-mode universal filter," *Indian J. Pure Appl. Phys.*, vol. 43, pp. 636–639, Aug. 2005.

[30] A. K. Singh and R. Senani, "CFOA-based state-variable biquad and its high-frequency compensation," *IEICE Electron. Exp.*, vol. 2, no. 7, pp. 232–238, 2005.

[31] N. A. Shah, S. Z. Iqbal, and M. F. Rather, "Versatile voltage-mode CFA-based universal filter," *AEU-Int. J. Electron. Commun.*, vol. 59, no. 3, pp. 192–194, Jun. 2005.

[32] V. K. Singh, A. K. Singh, D. R. Bhaskar, and R. Senani, "New universal biquads employing CFOAs," *IEEE Trans. Circuits Syst. II, Exp. Briefs*, vol. 53, no. 11, pp. 1299–1303, Nov. 2006.

[33] S. Topaloglu, M. Sagbas, and F. Anday, "Three-input single-output second-order filters using current-feedback amplifiers," *AEU-Int. J. Electron. Commun.*, vol. 66, no. 8, pp. 683–686, Aug. 2012.

[34] S. A. Mahmoud, A. H. Madian, and A. M. Soliman, "Low-voltage CMOS current feedback operational amplifier and its application," *ETRI J.*, vol. 29, no. 2, pp. 212–218, Apr. 2007.

[35] E. Yuce and S. Minaei, "A modified CFOA and its applications to simulated inductors, capacitance multipliers, and analog filters," *IEEE Trans. Circuits Syst. I, Reg. Papers*, vol. 55, no. 1, pp. 266–275, Feb. 2008.

[36] S. Nikoloudis and C. Psychalinos, "Multiple input single output universal biquad filter with current feedback operational amplifiers," *Circuits, Syst. Signal Process.*, vol. 29, no. 6, pp. 1167–1180, Dec. 2010.
[37] J. W. Horng, "Voltage-mode universal biquad with five inputs and two outputs using two current feedback amplifiers," *Indian J. Eng. Mater. Sci.*, vol. 20, pp. 87–91, Apr. 2013.
[38] C. Wang, J. Zhang, L. Wang, W. Shi, and D. Jing, "A novel nth-order voltage-mode universal filter based on CMOS CFOA," *Opt. Int. J. Light Electron Opt.*, vol. 127, no. 4, pp. 2226–2230, Feb. 2016.
[39] A. K. Singh and R. Senani, "Active-R design using CFOA-poles: New resonators, filters, and oscillators," *IEEE Trans. Circuits Syst. II, Analog Digit. Signal Process.*, vol. 48, no. 5, pp. 504–511, May 2001.
[40] W. Tangsrirat and W. Surakampontorn, "Single-resistance-controlled quadrature oscillator and universal biquad filter using CFOAs," *AEU-Int. J. Electron. Commun.*, vol. 63, no. 12, pp. 1080–1086, Dec. 2009.
[41] C. M. Chang, C. S. Hwang, and S. H. Tu, "Voltage-mode notch, lowpass and bandpass filter using current-feedback amplifiers," *Electron. Lett.*, vol. 30, no. 24, pp. 2002–2003, 1994.
[42] J. W. Horng and M. H. Lee, "High input impedance voltage-mode lowpass, bandpass and highpass filter using current-feedback amplifiers," *Electron. Lett.*, vol. 33, no. 11, pp. 947–948, 1997.
[43] N. A. Shan and M. A. Malik, "High input impedance voltage-mode lowpass, bandpass, highpass and notch filter using current feedback amplifiers," *Indian J. Eng. Mater. Sci.*, vol. 12, pp. 278–280, Nov. 2005.
[44] N. A. Shan and M. A. Malik, "New high input impedance voltage-mode lowpass, bandpass and highpass filter using current feedback amplifiers," *J. Circuits Sys. Comput.*, vol. 14, no. 6, pp. 1037–1043, 2005.
[45] S.-F. Wang, H.-P. Chen, Y. Ku, and P.-Y. Chen, "A CFOA-based voltage-mode multifunction biquadratic filter and a quadrature oscillator using the CFOA-based biquadratic filter," *Appl. Sci.*, vol. 9, no. 11, p. 2304, Jun. 2019.
[46] S.-F. Wang, H.-P. Chen, Y. Ku, and M.-X. Zhong, "Voltage-mode multifunction biquad filter and its application as fully-uncoupled quadrature oscillator based on current-feedback operational amplifiers," *Sensors*, vol. 20, no. 22, p. 6681, Nov. 2020.
[47] S.-F. Wang, H.-P. Chen, Y. Ku, and C.-L. Lee, "Versatile voltage-mode biquadratic filter and quadrature oscillator using four OTAs and two grounded capacitors," *Electronics*, vol. 9, no. 9, p. 1493, Sep. 2020.
[48] Y. Tao and J. K. Fidler, "Electronically tunable dual-OTA second-order sinusoidal oscillators/filters with non-interacting controls: A systematic synthesis approach," *IEEE Trans. Circuits Syst. I, Fundam. Theory Appl.*, vol. 47, no. 2, pp. 117–129, Feb. 2000.
[49] H.-Y. Wang, H.-D. Tran, Q.-M. Nguyen, L.-T. Yin, and C.-Y. Liu, "Derivation of oscillators from biquadratic band pass filters using circuit transformations," *Appl. Sci.*, vol. 4, no. 4, pp. 482–492, Sep. 2014.
[50] P. Andreani and X. Wang, "On the phase-noise and phase-error performances of multiphase LC CMOS VCOs," *IEEE J. Solid-State Circuits*, vol. 39, no. 11, pp. 1883–1893, Nov. 2004.

SAN-FU WANG was born in Changhua, Taiwan, in 1976. He received the M.S. and Ph.D. degrees from the Department of Electronic Engineering, Institute of Computer and Communication, National Taipei University of Technology, Taiwan, in 2003 and 2010, respectively. He is currently an Associate Professor with the Department of Electronic Engineering, Chin-Yi University of Technology, Taiwan. His research interests include mixed-signal integrated circuits and analog signal processing.

HUA-PIN CHEN received the M.S. and Ph.D. degrees from Chung Yuan Christian University, Taiwan, in 2001 and 2005 respectively. Since August 2009, he has been an Associate Professor with the Department of Electronic Engineering, Ming Chi University of Technology. He is currently a Professor with the Department of Electronic Engineering, Ming Chi University of Technology. His teaching and research interests include circuits and systems, analog and digital electronics, active filter/oscillator design current-mode integrated circuits, and current-mode signal processing.

YITSEN KU received the B.S. degree in electronics engineering from Tam Kang University, Taipei, Taiwan, in 1986, the M.S. degree in electrical engineering from California State University Fullerton, Fullerton, CA, USA, in 2005, and the Ph.D. degree from the National Taipei University of Technology, Taipei, in 2014. He is currently an Adjunct Professor with the Department of Electrical Engineering, California State University Fullerton. His current research interests include analog integrated circuits, current-mode integrated circuits, and current-mode analog signal processing.

MING-XIU ZHONG received the B.S. degree in electronic engineering from the Ming Chi University of Technology, New Taipei City, Taiwan, in 2019, where he is currently pursuing the M.S. degree. His research interests include IC circuits design and plastic circuit board design, which assists verifying the ability of IC circuits. He is also good at simulating circuits via MATLAB and OrCAD PSpice.